

# **Eruption-fed turbidity currents: their thermo-fluid dynamics and sedimentation from explosive subaqueous eruptions**

A. Cantelli

Dept. of Civil & Environmental Engineering & Dept. of Geology, University of Illinois, Urbana, Illinois, USA, cantelli@uiuc.edu

S. Johnson

Dept. of Civil Engineering, University of Minnesota, Minneapolis, Minnesota, USA, john3999@umn.edu

J.D.L. White

Geology Department, University of Otago, Dunedin, NZ, james.white@otago.ac.nz

G. Parker

Dept. of Civil & Environmental Engineering & Dept. of Geology, University of Illinois, Urbana, Illinois, USA, parkerg@uiuc.edu

**ABSTRACT:** Deposits of turbidity currents induced by subaqueous volcanic eruptions are increasingly recognized in settings ranging from lakes to the deep sea. These "eruption-fed density currents" have high current temperatures and low-density particles, which affect current dynamics and deposit features. Field data indicate that deposit thickness and grain size decrease downflow at a changing rate. This trend is similar for deposits of non-eruptive turbidity currents, but with volcanic activity, the deposits often exhibit a marked discontinuity in deposit thickness and grain-size distribution. Here we present laboratory results on density currents that address the effects of variations in grain density and water temperature on flow properties and depositional processes. Parallel runs were performed under identical flow conditions utilizing quartz sand and pyroclastic sediment. Each grain type was used in one series of runs in which a hot density current enters a cold environment, and one series in which a cold current enters a similarly cold environment. Experiments in which the inflow contained hot water and low-density sediment tended to emplace the deposit center of mass proximally; sedimentation also reduced bulk-current density below that of the ambient water, giving rise to a buoyant plume from which suspension sedimentation occurred. By contrast, experiments in which the inflow contained cold water and high-density sediment tended to deposit mass distally, with no accompanying plume. Results of the study have special relevance to submarine volcanoclastic deposits, but also illuminate fundamental aspects of how grain properties and water temperature affect the driving force of density currents.

keywords: density current, sediment gravity flow, submarine eruption, surtseyan, thermal plume, pyroclastic flow

## 1 INTRODUCTION

Volcanoclastic deposits formed by subaqueous density currents have been widely identified. Eruption-fed density currents have been inferred to play important roles in constructing subaqueous volcanoes (e.g. Fiske, 1963; Mueller and White, 1992; White, 1996; Smellie and Hole, 1997; Fiske et al., 1998; Smellie, 1999; White and Houghton, 1999; White, 2000). Turbidites composed of reworked ash and other volcanic debris also form large parts of marine arc successions (Dickinson, 1968; Robertson, 1984; Busby-Spera, 1985; Busby-Spera, 1986; Orton, 1996). Despite their abundance along volcanically active plate margins and their fundamental role in the construction of subaqueous volcanoes and the substructures of volcanic islands, subaqueous volcanoclastic density currents have rarely been investigated experimentally,

and no experiments have fully addressed the effect of heat or variable particle density on the currents' deposits.

Turbidity currents are a specific subset of density currents, differentiated by the fact that the density of the current is determined by the presence of suspended sediment. Because turbidity currents are considered responsible for various morphologic features in marine and lake environments, and because of their role in forming large proportions of earth's sedimentary rock, many aspects of turbidity currents have previously been studied. Many authors have examined the general concepts of density currents (e.g. Schmidt 1911; von Karman 1940; Keulegan 1957; Ellison & Turner 1959; Hinze 1960; Plapp & Mitchell 1960; Chu, Pilkey & Pilkey 1979; Lüthi 1981). Turbidity currents are driven by the downslope component of gravity pulling the suspended sediment, and thus the surrounding water, downstream. This suspended sediment is free to exchange with bed sediment. Depending upon conditions, turbidity currents can produce both net bed erosion and net bed deposition (Pantin 1979; Parker 1982; Garcia 1985).

Other parameters in addition to the concentration of suspended sediment in the water column control the dynamics of turbidity currents generated by volcanic eruptions under water. The water carrying the sediment is to varying extents heated by the eruption, and so tends to be hotter and hence of lower density than the ambient water. This tends to reduce the driving force of the turbidity current. In addition, particles produced by subaqueous eruptions tend to be of more varied, but generally lower, density than most natural sediments; they have highly angular shapes, are typically riddled with cavities (vesicles), and change density as the original eruption gases in the vesicles are replaced by water. Particle density and shape and current-water temperature are all important variables for turbidity current flow dynamics. Because eruption-fed currents exhibit extreme values for both current temperatures and particle shape and density, eruption-fed volcanoclastic deposits offer insight into both eruption-specific transport, and into wider issues regarding fundamental controls on density-current behavior.

In the subaerial environment, explosive volcanic eruptions produce primary pyroclastic deposits formed from eruptive fragmentation followed by single-stage transport through the ambient atmosphere. In contrast, many subaqueous explosive eruptions produce turbidity currents, which in turn produce deposits with diverse geometries. Various types of density currents generated by submarine volcanic eruptions have been described (White, 2000), with each type of current responsible for a unique set of depositional features. In particular, three main classes of density current exist, each associated with a different kind of eruption. The first comprises subaqueous pyroclastic flows, which are high-temperature and necessarily high-particle concentration gas-solid flows driven by the excess density of the current relative to the water. They are generated by eruptions generating sustained gas-thrust columns. The second, and most common, consists of eruption-fed turbidity currents comprising dilute to high concentration particulate gravity flows with water as the continuous intergranular phase. These form directly both from sustained subaqueous columns and from intermittent tephra jets. A third set involves lava-fed density currents characterized by a continuous water phase and low to high particle concentrations generated by fragmentation of lavas during rapid effusive eruption.

The purpose of this paper is to investigate the dynamics and the resultant deposits of turbidity currents generated directly from subaqueous volcanic eruptions. This is accomplished by analyzing data from a series of laboratory experiments using both regular sand and pyroclastic sediment, and involving inflowing water that may be either at the same temperature as or hotter than the ambient water.

## 2 EXPERIMENTAL SET UP

At the St. Anthony Falls Laboratory (University of Minnesota) a series of turbidity current experiments was performed in a 0.2 m wide and 9.5 m long channel suspended inside a larger glass-walled tank (main tank; Figure 1). The channel slope was fixed at 6 degrees. Exterior tank dimensions are 10 m long, 3 m high and 0.6 m wide. Experiments were performed by releasing turbidity currents from a head tank with a capacity of 200 liters by way of an automated gate with a width of 0.15 m and a height of 0.11 m. The bottom of the gate was flush with the bed of the channel. The head tank was filled with a slurry of water and sediment which was released to form the turbidity current. Before release it was constantly agitated in order to maintain the sediment in suspension. The initial water surface in the head tank was elevated with respect to that in the larger glass-walled tank. The resulting potential energy difference ensured that all currents behaved as wall jets just downstream of the gate. The evolution farther downstream of any given current depended upon conditions enumerated below.

Each current so created was quasi-continuous in the sense that flow from the head tank continued until the water surface in the head tank had equilibrated with the water surface in the main tank. The discharge from the head tank tended to decrease over time, however, in accordance with the decrease in the difference in water surface elevation. In each event the flow was typically sustained for 40 – 60 seconds.

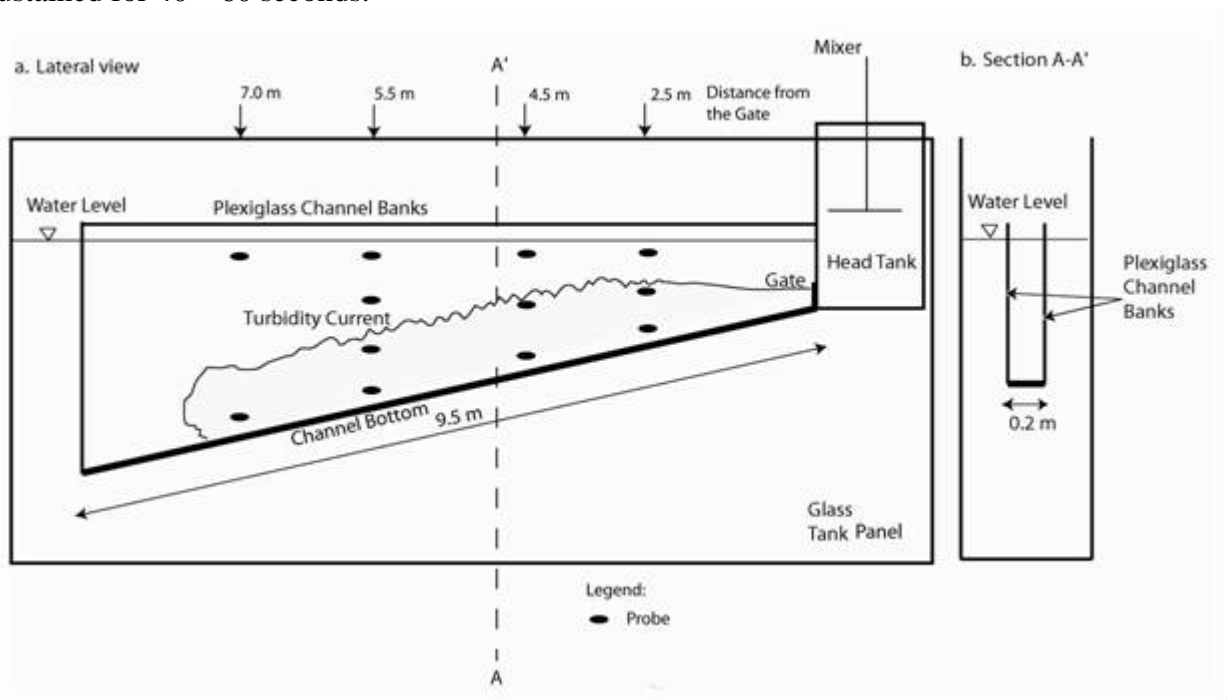


Figure 1. Facilities used at the St. Anthony Falls Laboratory.

Four series of runs were performed. Each series consisted of a number of turbidity currents with successive deposits stacked one on top of another. Each turbidity current in a series had the same input conditions. As shown in Table 1, two types of sediment (silica sand and pyroclastic volcanic ash) and two temperature conditions (no temperature difference between head tank water and main tank water, and head tank water that was 62°C hotter than the water in the main tank) yielded four series.

Of the four series, Series 1 corresponds most closely to a 'standard' turbidity current (i.e. one of non-eruptive origin) carrying siliciclastic material and Series 4 corresponds most closely to the result of an explosive volcanic eruption under water.

In order to investigate the thermodynamic evolution of the turbidity currents, three supplemental experiments were performed using temperature sensing equipment. These runs were performed using the same input conditions as Series 2 (experiment B) and Series 4 (experiment C), plus an additional experiment using only heated water with no sediment (experiment A). For these 3 series, twelve water resistant temperature sensors were placed underwater in the channel and attached to long fixed rods extending vertically downward from the water surface of the flume. The locations of these rods within the flume corresponded to the locations of the vertical sections at 2.5, 4.5, 5.5 and 7.0 meters from the inlet section. The locations were chosen based on our observations from previous experiments and on the necessity to optimize the positions of the twelve sensors. In particular the first and second sections (2.5 m and 4.5m) contain three probes each, two of which are placed at 0.1 meters from the surface and the bottom and one at a midpoint of the two. The third section (5.5m) contains four probes with similar configuration to the others and the last one (7.0 m) contain two probes one at 0.1 meters from the surface and the bottom. Figure 1 illustrates the positions of the probes.

Table 1. Summary of the experiments performed.

<b>SERIES</b>	<b>Runs</b>	<b>Sediment</b>	<b><math>\Delta T</math> *</b>	<b><math>R_t</math></b>
<b>1</b>	<b>5</b>	<b>Silica Sand</b>	<b>0 C</b>	<b>0.02045</b>
<b>2</b>	<b>5</b>	<b>Silica Sand</b>	<b>62 C</b>	<b>0.0016</b>
<b>3</b>	<b>3</b>	<b>Pyroclastic</b>	<b>0 C</b>	<b>0.00763</b>
<b>4</b>	<b>3</b>	<b>Pyroclastic</b>	<b>62 C</b>	<b>-0.01103</b>
<b>A</b>	<b>1</b>	<b>None</b>	<b>62 C</b>	<b>-0.04796</b>
<b>B</b>	<b>1</b>	<b>Silica Sand</b>	<b>62 C</b>	<b>0.0016</b>
<b>C</b>	<b>1</b>	<b>Pyroclastic</b>	<b>62 C</b>	<b>-0.01103</b>

\*Temperature difference between the turbidity current slurry in the head tank and the ambient water temperature in the main tank

Most volcanoclastic sediment grains have vesicles, rendering the grains porous and permeable to varying degrees. Rates of water saturation for the vesicular clasts are mediated by inhomogeneities in the vesicle population, and in particular by more rapid transport of water through larger vesicles into the interiors of the clasts (Manville et al., 1998). Experimental studies show that highly vesicular clasts (pumice) eventually become saturated with water, but retain slightly lower bulk densities than smaller clasts due to the effects of small volumes of non-connected pore space that remains open. In general, however, fall velocities are proportional to grainsize for water-saturated vesicular clasts (Tilly, 1987; Manville et al., 1998). Sorting of saturated pumice by fall velocity produces normally graded pumice beds ("redeposition grading"; White et al., 2001). Subaqueous entrainment of pumice clasts takes place at low bed shear stresses, and deposition of pumice from currents results in a range of conventional styles of crossbedding, as well as producing distinctive steeply imbricated clast fabrics developed by the progressive growth of bedload cluster bedforms (Manville et al., 2002). Hot pumice, introduced by eruption or transport directly into water, may become immediately saturated with water (Whitham and Sparks, 1986). We will not directly address this behavior, which results from initial condensation of intragranular steam, but such "instant saturation" of subaqueously erupted vesicular particles means that experiments utilizing saturated clasts adequately represent eruption-fed density currents.

The sediment used in this set of experiments was collected from Pahvant Butte volcano, Utah, which was formed by subaqueous eruption into Lake Bonneville (Gilbert, 1890; White, 1996). Common silica sand has a specific dry density of  $2650 \text{ kg/m}^3$ , but this pyroclastic sediment averages  $2230 \text{ kg/m}^3$ . This difference can be explained by the vesicularity (air pockets within grains of dry sediment) of pyroclastic sediment which is typical of material of volcanic origin. Though not addressed by the experiments reported here, it is of value to note that during a subaqueous eruption particles would initially all have vesicles filled with gas. Particle cooling and vapor condensation rapidly draw water into open vesicles, but some internal vesicles commonly remain as open cavities contributing to reduced particle density (Whitham and Sparks, 1986; Manville et al., 1998).

In order to compare the effect of the two very different kinds of sediment, the silica sand was sieved to closely match the grain size distribution of the pyroclastic material. Figure 2 illustrates the comparison between the grain size distributions of the two sediments.

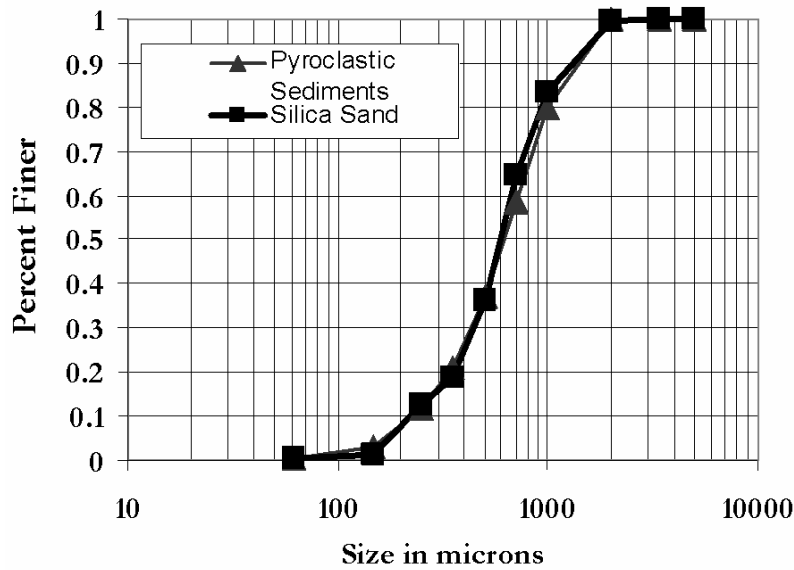


Figure 2. Grain size distributions of the silica sand the pyroclastic sediment.

The temperature difference between a sediment-laden current and the ambient water can be an important variable for turbidity currents in general, but is particularly important in the case of turbidity currents fed by volcanic eruptions, where the difference can be quite substantial (White, 2000). Let  $\Delta T$  denote the temperature difference between the water in the head tank and ambient water in the main tank. The water was heated with an electric element inside the head tank until the desired temperature was obtained. In two of the series  $\Delta T$  was zero; in the other two  $\Delta T$  was set equal to  $62^\circ\text{C}$ . That is, the water in the head tank was maintained  $62^\circ\text{C}$  hotter than the ambient water in the main tank. Though the range of initial temperatures in the field is an order of magnitude higher than that possible in the laboratory, the difference used here is sufficient to capture important aspects of the dynamics of field scale turbidity currents in relatively shallow water. This is because heat is transferred very rapidly from particles initially at c.  $1200^\circ\text{C}$  to water (e.g. Gudmundsson, 2003), yielding water at sub-boiling temperatures for turbidity currents arising from the eruption. For deep-water eruptions, initial current temperatures could potentially be several times higher because of pressure-induced elevation of the boiling point (e.g. Maicher et al., 2000), but we expect that they would remain dynamically similar to the currents addressed here.

Data acquisition consisted of measuring water temperature in the exterior main tank/channel and in the head tank before each run, capturing video of the advancing turbidity currents using a combination of four synchronized video cameras, measuring deposit profiles using a point gage, acquiring a series of digital images from the side of the channel after each run, and capturing underwater digital photographs from above the channel in order to examine bedforms. All of the images were corrected for optical distortion using appropriate software. In addition, runs A, B, and C were specifically designed to map the temperature change inside the tank during the runs. Twelve temperature measuring probes were used for this purpose.

### 3 CALIBRATION OF THE INITIAL CONDITIONS

Water temperature strongly affects the movement of and deposition from turbidity currents, particularly when there is no salinity contrast between the current and the ambient water (Allen, 1997). For example, glacier-fed cold underflows endure until mixing and diffusion destroy their density contrast with surrounding water (e.g. Chikita et al., 1997). Density underflows currents composed of water warmer than the ambient standing water must be driven by excess density provided by suspended sediment (Stolzenbach and Harleman, 1971). Some rivers entering the ocean are occasionally capable of generating warm density underflows (Mulder and Syvitski, 1995), but most cannot; very high sediment concentrations are necessary to overcome the buoyancy of warm, fresh water entering a cool basin with a salinity typical of the ocean. In subaqueous volcanic eruptions, both heat and particulate debris are mixed into surrounding water. Bottom density currents resulting from the addition of particles must overcome some buoyancy of the entraining fluid that results from addition of heat. As the current evolves, it loses heat and sediment particles; the balance between these two mechanisms determines whether the current eventually cools and runs out as a typical sediment-gravity flow, or whether it lofts from the depositional surface as a buoyant plume (e.g. Sparks et al., 1993, McLeod et al., 1999).

The fluid buoyancy effect is initially overcome by the density of the sediment fraction of the turbidity current. By determining a specific balance between sediment concentration and water temperature, it is possible to create a turbidity current with the following behavior: it exits the head tank with a sediment concentration that is sufficient to maintain downslope flow and attachment to the bottom. Farther downslope, as sediment is lost through deposition, the density difference between the current and the ambient water decreases, and eventually reverses near a point where the suspension detaches from the bottom of the channel and rises upward as a hot, buoyant but sediment-laden plume.

Because this effect is inevitable during the full runout of a natural volcanic current, reproducing this behavior in the laboratory setting is essential in order to investigate the effect of the temperature difference on the resultant deposit.

In Figure 3a the effect of temperature on water density is plotted. The density of a turbidity current,  $\rho_{tc}$ , is a function of the water density  $\rho_w$ , sediment density,  $\rho_s$ , and the sediment volume concentration,  $C$ , as follows:

$$\rho_{tc} = \rho_w(1 - C) + \rho_s C = \rho_w \left( 1 + \frac{\rho_s - \rho_w}{\rho_w} C \right) \quad (1a)$$

Now let  $\rho_{wh}$  denote the density of hot water in the head tank,  $\rho_{wa}$  denote the density of (ambient) cold water in the main tank and  $C_h$  denote the volume sediment concentration in the head tank. The fractional density difference  $R_t$  between the particulate-water mixture in the head tank and the ambient water in the main tank is given as

$$R_t = R_{th} + R_{rs} \quad , \quad R_{th} = \frac{\rho_{wh} - \rho_{wa}}{\rho_{wa}} \quad , \quad R_{rs} = \frac{\rho_s - \rho_{wh}}{\rho_{wa}} C_h \quad (2a,b,c)$$

In (2a) the term  $R_{th}$  represents the part of the fractional density difference due to the difference in temperature between the water in the head tank and the ambient water in the main tank. In the experiments reported here this term was either zero (Series 1 and 3) or negative (Series 2, 4, A, B and C). The term  $R_{rs}$  (2b) represents the fractional density difference associated with the presence of suspended particles in the head tank. This term was positive in all the experiments reported here except Series A, where it was zero.

Figure 3a and (2) were used to construct the relations shown in Figure 3b for  $R_t$  as a function of  $C_h$  for the experiments of Series 1, 2, 3 and 4. Figure 3b was in turn used to select a common value of  $C_h$  for the experiments with particulate matter. After a number of trial runs, a common value of  $C_h$  of 0.03 was selected for all the experiments reported here in which particulate material was added (i.e. all series except Series A). The values of  $R_t$  are reported in Table 1.

The downstream evolution of the current emanating from the head tank depended on the values of  $R_{th}$  and  $R_{rs}$ . When  $R_{th} < 0$  and  $R_{rs} = 0$  (Series A), the current ran out for a very short distance as a wall jet attached to the channel bed, but then detached and rose upward as a hot, buoyant plume. When  $R_{th} = 0$  and  $R_{rs} > 0$  (Series 1 and 3) the current transformed from a wall jet to a bottom density flow, and ran out along the channel bed as a net-depositional turbidity current with no detachment. When  $R_{th} < 0$ ,  $R_{rs} > 0$  and  $R_t = R_{th} + R_{rs} > 0$  (Series 2 and B) the current transformed proximally from a wall jet to net-depositional turbidity current, and then detached distally to form a buoyant plume as the particulate driving force was lost to deposition.

Series 4 and C corresponded to the conditions  $R_{th} < 0$ ,  $R_{rs} > 0$  and  $R_t = R_{th} + R_{rs} < 0$ . Since the water-particle mixture in the head tank was lighter than the ambient water in the main tank it might be expected that the wall jet emanating from the gate should have transformed directly into a buoyant (albeit sediment-laden) plume. The observed behavior was, however, rather more complex. The upper part of the wall jet did indeed transform into a buoyant plume. The tendency for sediment to settle, however, resulted in an elevation in particulate concentration in the lower part of the jet that was sufficient to cause it to transform into a turbidity current. This turbidity current then detached farther downstream to form a second buoyant plume as the particulate driving force was lost to deposition.

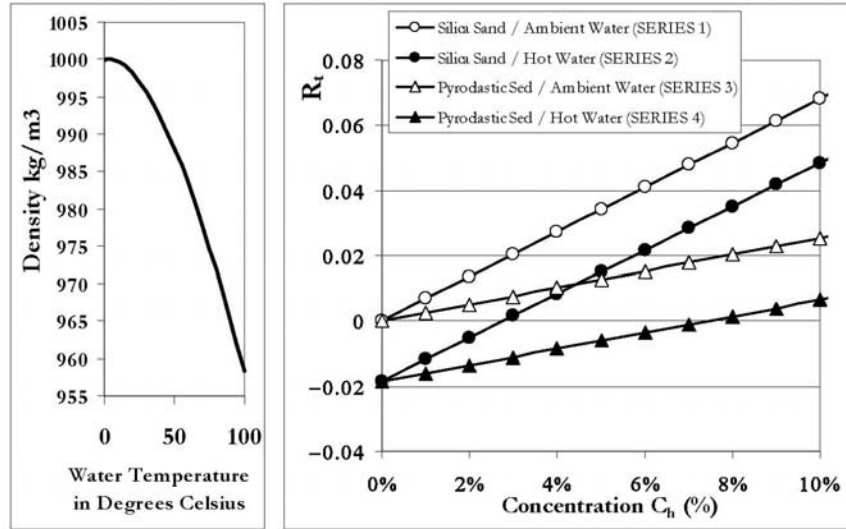


Figure 3a. Relation between density of particulate-free fresh water and water temperature.

Figure 3b. Fractional excess density  $R_t$  of a turbidity current as a function of the volume sediment concentration  $C_h$ . The four cases plotted correspond to a) silica sand with  $\Delta T = 0^\circ\text{C}$  (ambient and head tank at  $12^\circ\text{C}$ ); b) silica sand with  $\Delta T = 62^\circ$  (ambient water at  $12^\circ\text{C}$  and head tank at  $74^\circ\text{C}$ ); c) pyroclastic material with  $\Delta T = 0^\circ\text{C}$  (ambient and head tank at  $12^\circ\text{C}$ ) and d) pyroclastic material with  $\Delta T = 62^\circ\text{C}$  (ambient water at  $12^\circ\text{C}$  and head tank at  $74^\circ\text{C}$ ).

## 4 EXPERIMENTAL RESULTS.

### 4.1 Thermal effects on the evolution of turbidity currents

The runs of Series 1 and 3 (for which  $\Delta T^\circ = 0$ ) are referred to as “cold runs”, and the runs of Series 2 and 4 (for which  $\Delta T^\circ = 62^\circ$ ) are referred to as “hot runs”.

Figure 4a shows the head and part of the body of a turbidity current from a cold run of Series 3, for which  $\Delta T = 0$ . The current flowed downslope, always attached to the bottom of the channel. This current, while strongly depositional in nature, ran the entire 10 m of the tank. Figure 4b shows a turbidity current from a hot run Series 2, for which  $\Delta T = 62^\circ$ ; the effect of the temperature difference is visible from the interface that divides the hot turbidity current from the clear cold water. The hot turbidity current of Figure 4b detached from the bottom of the channel approximately 4.5 m downstream from the inlet gate, feeding a plume that contained a low concentration of suspended sediment. This plume rose to the water surface, and the fine suspended material carried with it gradually rained out onto the bed.

The turbidity currents of the hot runs (Series 2 and 4) showed patterns of downstream variation in head or front velocity that differ significantly from those of cold runs (Series 1 and 3). The velocity of the flow front, was determined from measurements of the position and time of the front. Let  $X$  denote a down-channel streamwise coordinate,  $Z$  denote a coordinate upward-normal to the bed, as shown in Figure 5, and  $V_X$  and  $V_Z$  denote the values of head velocity in the corresponding directions. Figure 5 shows the downstream variation in  $V_X$  and  $V_Z$  for the first run of Series 1 ( $\Delta T = 0^\circ$ ; cold current) and the first run of Series 2 ( $\Delta T = 62^\circ$ ; hot current).

In the case of the cold current, the streamwise front velocity  $V_X$  was everywhere positive. Although the value of  $V_X$  gradually declined downstream, it was still positive at the downstream end of the tank. In addition, the upward normal front velocity  $V_Z$  was essentially vanishing everywhere, indicating that the current remained attached to the bed. In the case of the hot

current,  $V_x$  was everywhere lower than the corresponding value for the cold current, dropping to nearly zero near  $X = 4.55$  m. In addition,  $V_z$  was nearly vanishing up to  $X = 4.55$  m, but farther downstream  $V_z$  became positive. That is, the hot current lifted off the bed at  $X = 4.55$  m, a location that is here called the “detachment point”. Head propagation velocities were consistent in trend as well as order of magnitude for all runs in the series.

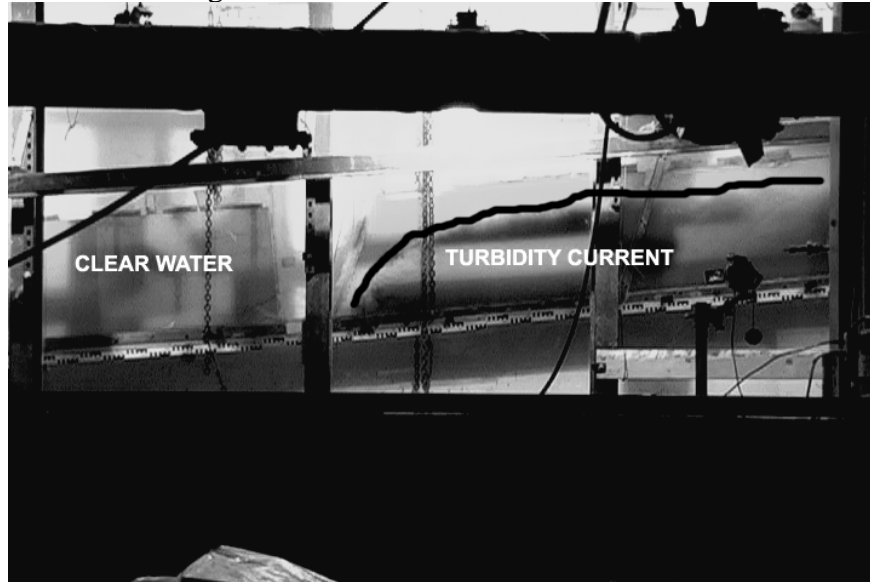


Figure 4a. The head of a turbidity current with no temperature difference (SERIES 3 run a,  $\Delta T = 0^\circ$ ) remains attached to the bottom of the channel. The flow is from right to left. The black line was inserted to illustrate the approximate boundary between clear water and sediment-laden water..



Figure 4b. A turbidity current with an upstream temperature difference  $\Delta T$  of  $62^\circ$  tends to billow upward as it propagates downslope (SERIES 2 run a). The flow is from left to right. The black line was inserted to illustrate the approximate boundary between clear water and sediment-laden water. Note that although the bed slopes to the left, the interface between the sediment-laden and clear water slopes to the right.

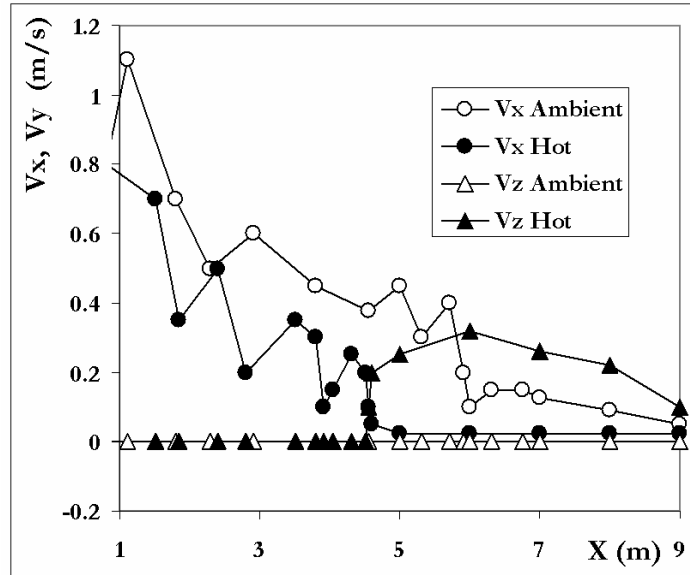


Figure 5. Diagram showing the downstream variation in the streamwise and upward normal components of head (front) velocity ( $V_x$  and  $V_z$ , respectively). The open symbols pertain to a cold current (Run 1 of Series 1, for which  $\Delta T = 0^\circ$ ), and the closed symbols pertain to a hot current (Run 1 of Series 2, for which  $\Delta T = 62^\circ$ ).

The turbidity currents were net depositional in all runs. Analysis of the resultant deposits illustrates different features formed in response to temperature difference and sediment type.

#### 4.2 Thermal effect on the resultant deposit

Figure 6 shows downstream profiles of deposit thickness for the third run (c) of each of Series 1, 2, 3 and 4.

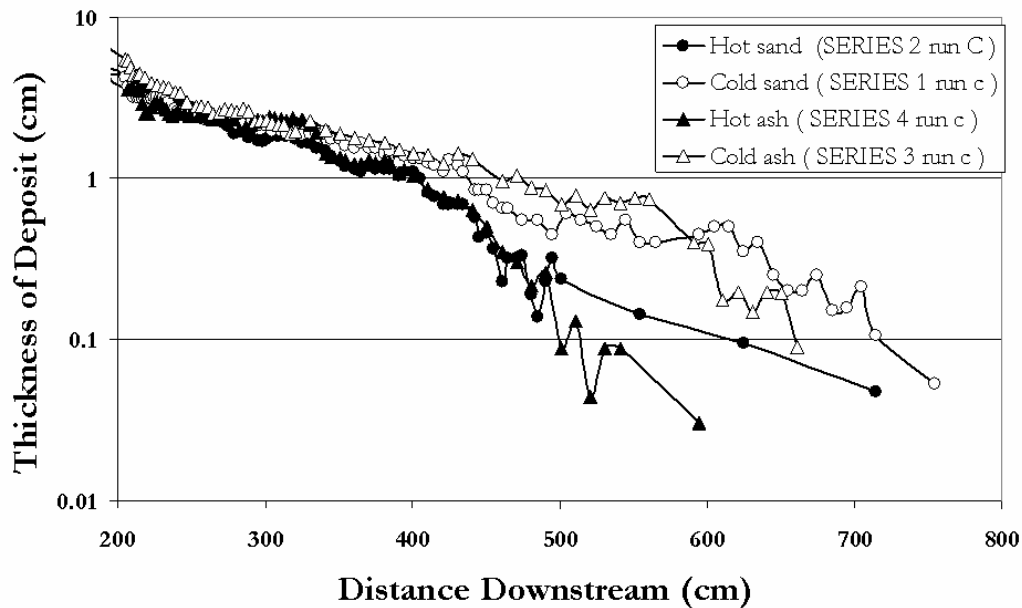


Figure 6. Deposit profiles for the third run (c) of each series.

Deposit thickness is plotted starting 2 m downstream of the inlet gate so as to exclude the region where the flow behaved as a wall jet. The plots are truncated at a thickness of about 0.05 cm only because thinner deposit thicknesses could not be accurately measured. In all cases, however, the entire length of the channel was covered with at least a thin layer of sediment.

For each deposit, the thickness decreased with distance down the flume. It is apparent from Figure 6 that for each sediment type, deposit thickness declined more rapidly downstream in the case of the hot flows ( $\Delta T = 62^\circ$ ). The difference is particularly strong downstream of  $X = 450$  cm. This illustrates the tendency of the temperature difference to arrest the current and cause detachment not far downstream of this point. The difference in deposit structure between hot and cold flows was stronger in the case of the volcanic ash than in the case of the silica sand. A weaker, but still discernible difference in deposit structure is also evident in comparing different sediment types at the same temperature difference. The very distal deposit thickness for the flow with volcanic ash is less than that for the corresponding flow with silica sand. Both trends are expected; hot water tends to arrest a turbidity current, and volcanic ash is of lower density than silica sand, yielding a weaker downslope gravitational force acting on the current.

The long profile of deposit thickness for each run was used to compute a streamwise position  $X_c$  of the center of mass of the deposit. A small value of  $X_c$  implies that the sediment was deposited more proximally (weaker turbidity current) and a large value of  $X_c$  implies that the sediment was deposited more distally (stronger turbidity current). Figure 7 demonstrates that this center of mass was consistently displaced upstream in the hot runs (Series 2 and 4) as compared to the cold runs (Series 1 and 3).

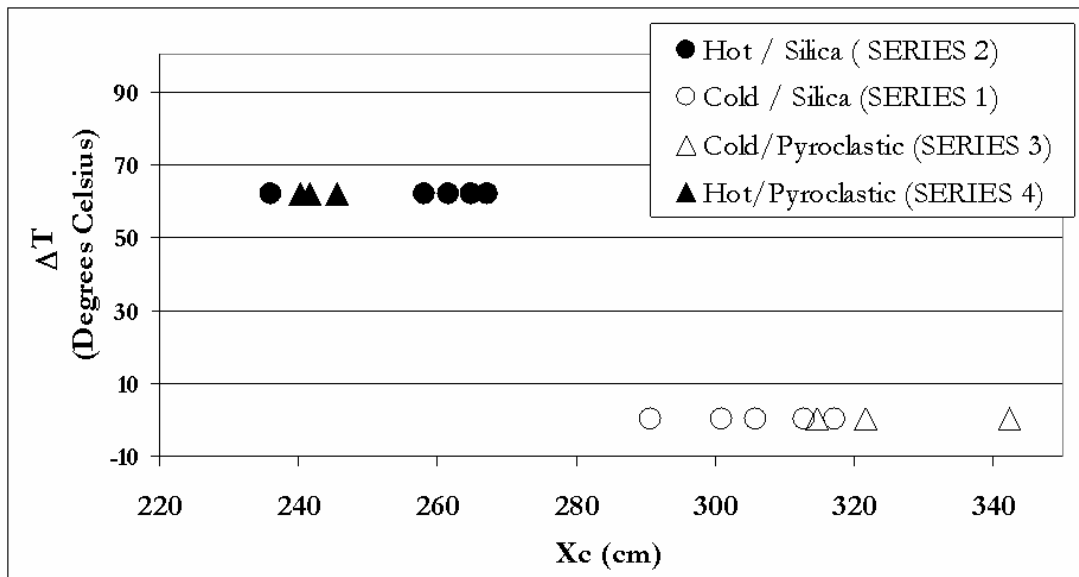


Figure 7. Center of mass  $X_c$  of the deposit as a function of temperature difference  $\Delta T$ . Here circles represent silica sand runs, triangles represent pyroclastic sediment runs, open symbols denote cold runs ( $\Delta T = 0^\circ\text{C}$ ) and black symbols denote hot runs ( $\Delta T = 62^\circ\text{C}$ ).

#### 4.3 Thermal effect on grain size distribution along the deposit

The deposits showed a tendency for characteristic grain size to decrease downstream.

Figure 8 shows the grain size distributions of the bed samples taken at various positions along the flume. The upstream reach of the flume between  $X = 0$  and  $X = 1.5$  m was not sampled, as this region was strongly affected by the wall jet emanating from the head gate. The plots in Figure 8 are from Series 1, 2, 3 and 4; the tendency for downstream fining.

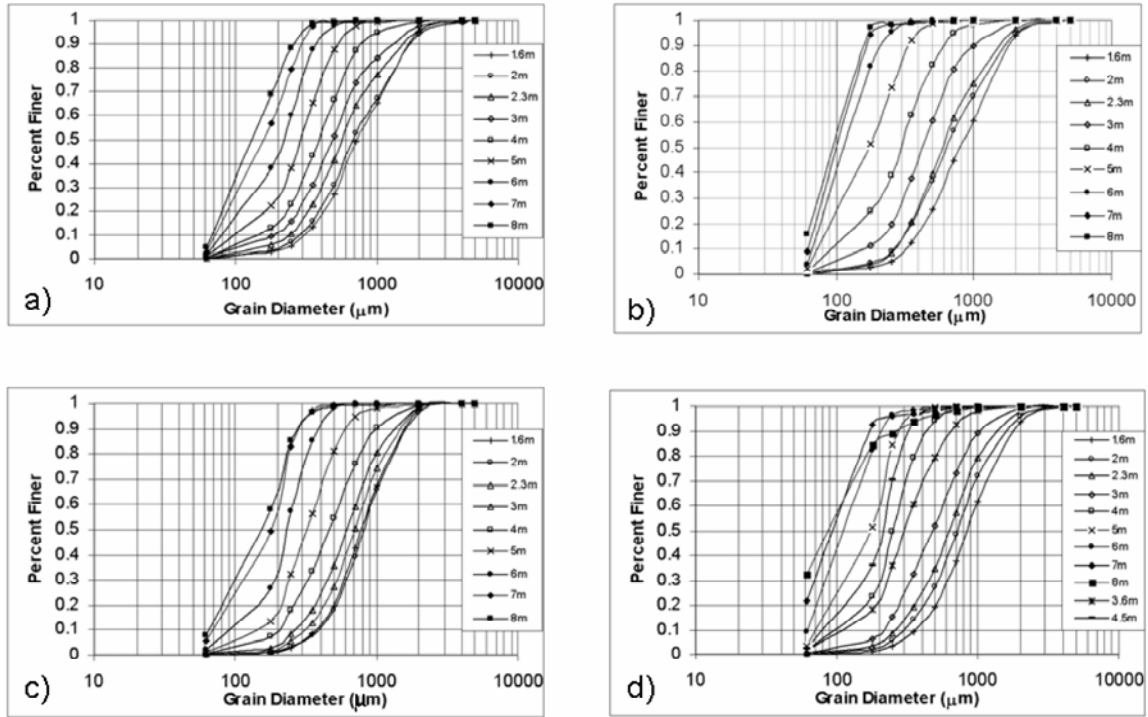


Figure 8. Grain size distributions for the bed samples at different streamwise locations along the flume. Streamwise location is characterized in terms of distance downstream of the gate of the head box. Plot a) pertains to the turbidity currents from Series 1 (cold silica), plot b) to those from Series 2 (hot silica). plot c) to those from Series 3 (cold pyroclastic) and plot d) to those from Series 4 (hot pyroclastic).

Comparison of the grainsize distributions from the samples taken at different distances along the flume from the headtank show a persistent downstream fining of the material.

In figures 9 a), b), and c), the 10<sup>th</sup> (D10), 50<sup>th</sup> (D50), and 90<sup>th</sup> (D90) cumulative percentile values for the samples are plotted against the streamwise locations of the samples. Values are calculated for Series 1, 2, 3, and 4. Contrary to the standard procedure, the plots are presented in terms of a linear, rather than logarithmic scale for grain size in order to emphasize several structures in the deposit noted below.

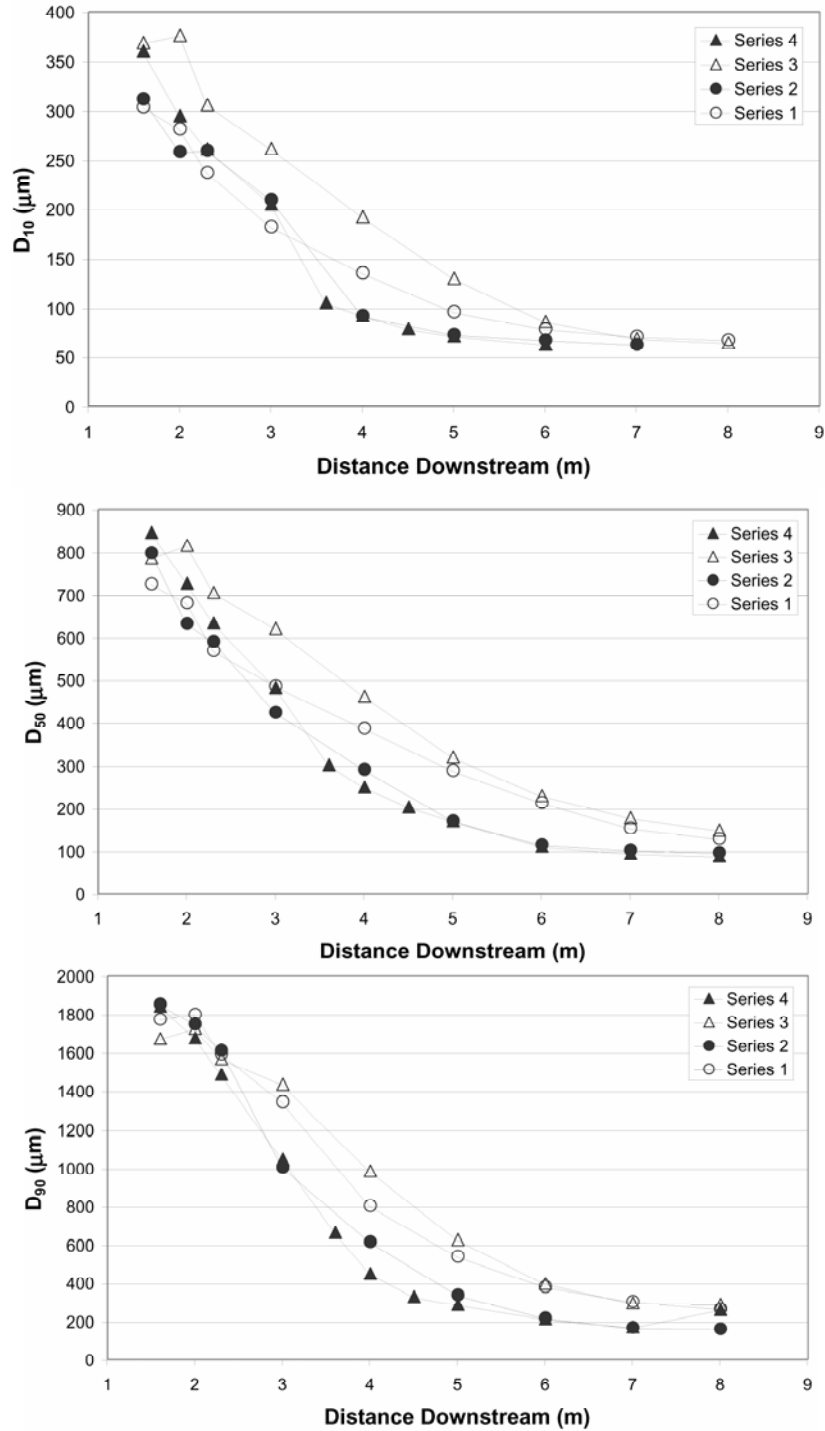


Figure 9.  $D_{10}$ ,  $D_{50}$ , and  $D_{90}$  values for the deposit as functions of distances downstream of the inlet for the experiments of Series 1, 2, 3, and 4. Solid symbols denote hot-current series, open symbols denote cold-current series; triangular symbols represent runs with pyroclastic sediment and circular symbols represent the runs with silica sand.

Figure 9 allows a clear distinction between the hot runs (Series 2 and 4) and the cold runs (Series 1 and 3). Consider a “proximal zone” extending from 2 m to about 4.5 m downstream of the

head box, and a “distal zone” extending from about 5.5 m to 8 m downstream of the head box. The proximal deposits of the hot runs (solid symbols) show a more rapid rate of downstream fining than those of the cold runs (open symbols), as manifested in the downstream change in  $D_{90}$ ,  $D_{50}$  and  $D_{10}$  of the deposits. In the distal region the deposits of the hot runs are finer than those of the cold runs, but also show a lower rate of downstream fining.

This behavior is another manifestation of the tendency of the temperature difference of the hot runs to arrest the currents. The upward detrainment of hot water in a hot run weakens the turbidity current in the downstream direction, forcing it to deposit coarser material at a higher rate in the proximal zone than the corresponding cold run. Downstream of about  $X = 4.5$  m, however, the currents of the hot runs detach, carrying very fine-grained material upward. The buoyant plume rises upward and then spreads both upstream and downstream of the detachment point; the fine material carried by the plume gradually rains out to form a thin layer over the length of the deposit. Upstream of the detachment point, this thin layer caps a much thicker layer emplaced by the turbidity current. Downstream of the detachment point, however, this layer of very fine material constitutes the totality of the deposit. Very fine material deposited in this way shows little downstream variation in grain size. In the case of the cold runs, however, the sediment deposits distally from a gradually weakening (rather than arrested) turbidity current, resulting in a continuation of the pattern of downstream fining observed in the proximal region.

The curves for the hot runs of figure 9 thus display a discontinuity that is not present in those of the cold runs. This discontinuity is perhaps best seen in figure 9b, which shows the downstream variation of the median size  $D_{50}$  of the deposit. For all points  $\leq 5$  m,  $D_{50}$  for both hot runs is seen to decrease downstream, whereas for all points  $\geq 6$  m,  $D_{50}$  is seen to be nearly constant for both hot runs. The cold runs of figure 9b do not display this discontinuity, which can be interpreted as a depositional signal distinguishing a hot run from a cold run.

This discontinuity associated with the hot runs is evident not only from the grain size distributions themselves, but also from the visual texture of the surface deposit. Figure 10 shows a photograph of the deposit of Run 4 (hot run; volcanic ash) downstream of the detachment point, alongside a corresponding photograph of the deposit of Run 3 (cold run; volcanic ash), in which there was no detachment. The rain of fine-grained material from the buoyant plume in the case of Run 4 renders the bed deposit visibly finer and smoother than that of Run 3.

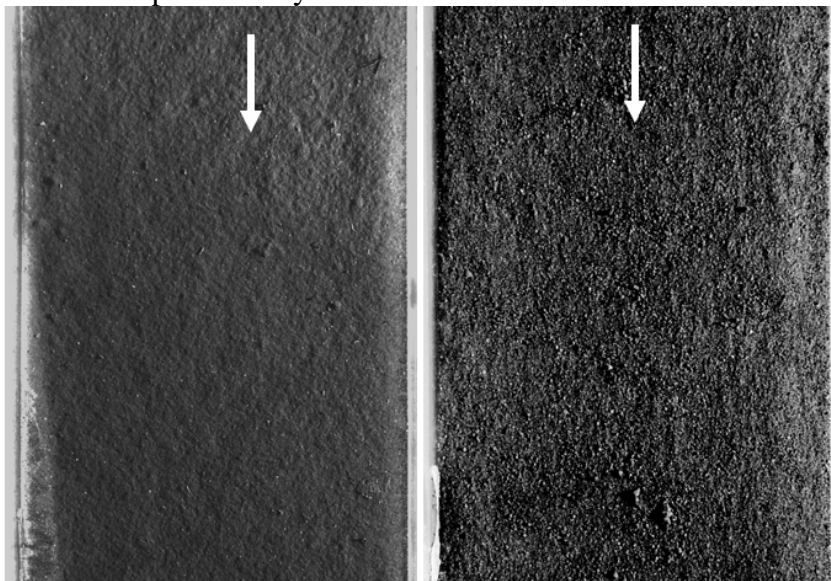


Figure 10. The image on the left shows the deposit of Run 4 (hot run; pyroclastic material) downstream of the detachment point. The image on the right shows the deposit of Run 3 (cold run; pyroclastic material) over the same reach as the image on the left. There was no detachment in the case of Run 3. The arrows denote the direction of the flow. In both images the width shown is the width of the channel, i.e. 0.2 m.

The patterns in Figures 8 - 10 have field analogs. In particular, field observations at Pahvant Butte and Black Point volcanoes (White, 1996; White, 2000) show relatively steep-sided accumulations of beds that nevertheless have shallow dips; the inference is that abruptly terminating beds are stacked up near the underwater vent, with an abrupt transition outward to much lower depositional rates producing thin and fine-grained beds of wide dispersal. At Black Point (Figure 11) this transition is reflected in a change, over less than 1 km laterally, from a near-source deposit comprising ~200 m of thick beds of gravelly sand-grade ash to a <5 m thick one of ripple-laminated silty sand-grade ash (White, 2000).

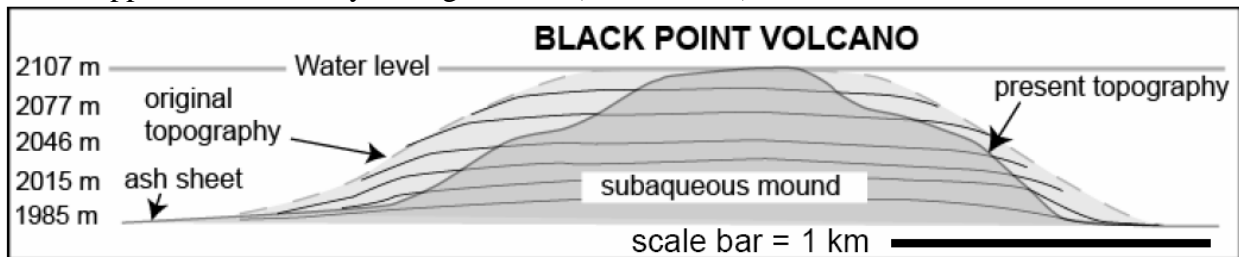


Figure 11. Inferred original form of Black Point volcano in cross-section. Thin lines illustrate shallow-dipping beds in mound. Steps in present topography result from wave erosion at different levels of the lake as it fell from syn-eruptive water level (labeled) to its current level of ~1955 m. Note the external slopes that are steeper than most bedding in the mound; the ash sheet is less than 10 m thick where arrowed, and remains ~ 3 m thick as far as 10 km from the volcano.

#### 4.4 Patterns of temperature variation in a hot run

In Runs 1 – 4 of Table 1, no attempt was made to measure patterns of temporal and spatial variation in water temperature during the course of the runs. Three more runs, i.e. Runs A, B and C of Table 1 were conducted in order to study temperature variation. Run A was identical to Runs 2 and 4 with the exception that the hot water was sediment-free. Run B was a repeat of Run 2, and Run C was a repeat of Run 4.

Four rakes of temperature probes were placed in the channel. These rakes were oriented vertically with their bottom ends adjacent to the positions  $X = 2.5$  m, 4.5 m, 5.5 m and 7 m. Each rake included one probe located 0.1 m above the bed (bottom probe) and another probe located 0.1 m below the water surface (top probe). In addition, each of the rakes at  $X = 2.5$  m and 4.5 m contained a third probe midway between the bottom and top probes, and the rake at  $X = 5.5$  m contained two more probes equally spaced between the bottom probe and the top probe. This configuration is shown in Figure 1. The probes were connected to a storage module which was in turn connected to a data logger. This data logger was used to set the desired rate of data collection from the probes and export this data to a computer. Temperatures at all probes were logged every second for the duration of a run. In addition, the timer of the data logger was synchronized with the timer of a still camera which recorded a side view of the flow. After the first ten minutes from the beginning of a run (by which time the flow had long ceased) the rate of data acquisition was changed to every ten seconds for the remaining twenty minutes, or until the data logger was full. For each experiment, over 1500 temperature values were collected using twelve sensors. The point data were interpolated in order to obtain a map of the temperature

distribution in the entire measurement domain for each time. Isotherms were interpolated from the data using Local Polynomial Interpolation (LPI), a moderately quick interpolation scheme that yields smooth curves. (Fan J. and Gijbels I., 1996). These maps allowed a graphical analysis of the density current and facilitated comparison of the flows produced in the runs.

Only results from Run C (hot run with pyroclastic material) are presented here. The tank itself is shown in the top panel of figure 12. Also shown in figure 12 are a) the flume itself and b) the temperature distribution within the flume at times corresponding to 8, 12, 17, and 20 seconds from the beginning of the experiment. (as noted above, run out duration varied from 40 – 60 seconds).

At  $t = 8$  seconds, the hot, particulate-laden water has displaced nearly all of the ambient water in a proximal zone near the head gate. The isotherms indicate that much of the hot water immediately flows toward the water surface, as would be expected from the value of  $R_t$  given in Table 1. At  $t = 12$  seconds, the isotherms near the current front are nearly vertical, and the current has propagated farther into the ambient fluid. By  $t = 20$  seconds the isotherms have rotated to become more nearly horizontal, indicating that the hot inflowing water is essentially flowing over the ambient water downstream of a detachment point.

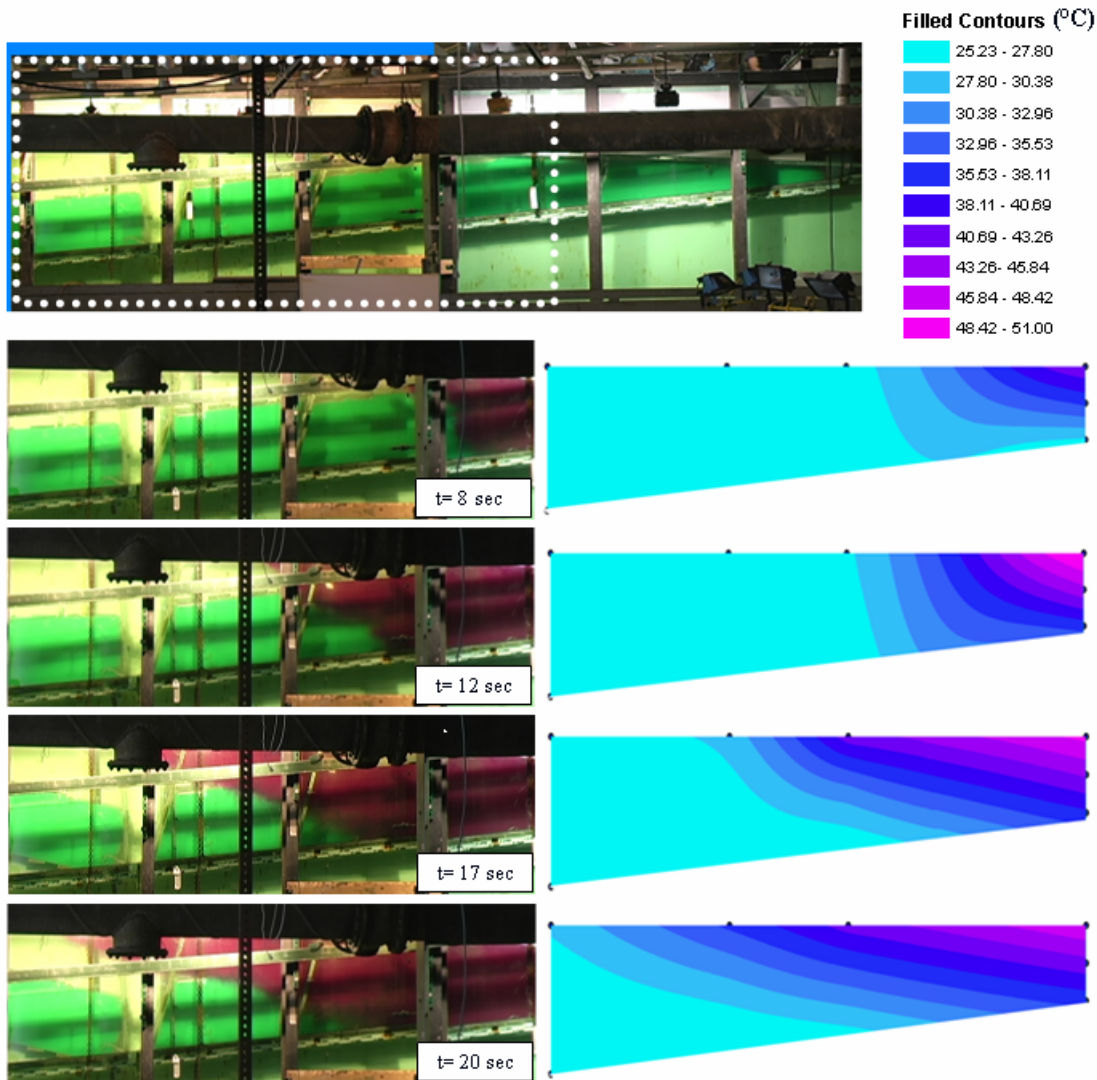


Figure 12. The top frame shows the tank for Run C. The four succeeding frames below show a) the tank (left) and b) a map of temperature distribution (right) for the times  $t = 8, 12, 17$  and  $20$  seconds, respectively. The flow is from right to left. The inflowing hot water is dyed to allow for visualization. Temperature is given in  $^{\circ}\text{C}$ , and ranges from about  $25^{\circ}\text{C}$  (light blue) to about  $51^{\circ}\text{C}$  (purple). The temperature interval from one color bar to the next represents a span of about  $2.6^{\circ}\text{C}$ .

#### 4.5 Estimated limiting particle concentration

In order for a particulate-laden hot water flow to continue to run out as a bottom density current in colder ambient water, the particulate-water mixture in the flow must be denser than that of the ambient water. Equation (1a) can be used to determine the minimum concentration  $C_{\min}$  which satisfies this condition. Let  $T_a$  denote the temperature of the ambient water in the tank,  $\rho_{wa}(T_a)$  denote the corresponding density of the ambient water,  $T_f$  denote the temperature of the flowing water and  $\rho_w(T_f) < \rho_{wa}(T_a)$  denote the corresponding density of the water in the sediment-water underflow. The concentration  $C_{\min}$  at which the density of the flowing water-sediment mixture becomes equal to that of the ambient water is given from equation (1a) as

$$C_{\min} = \frac{\rho_{wa}(T_a) - \rho_w(T_f)}{\rho_s - \rho_w(T_f)} \quad (3)$$

where  $\rho_s$  denotes the effective density of the sediment.

The experiments of Series 1, 2, 3 and 4 were performed during the summer, when  $T_a$  was close to  $24^{\circ}\text{C}$ . The experiments of Series A, B and C were performed in winter when  $T_a$  was close to  $12^{\circ}\text{C}$ . Figure 13 shows plots of  $C_{\min}$  versus  $T_f$  for a) ambient water at  $0, 12$  and  $24^{\circ}\text{C}$  and b) sediment densities  $\rho_s$  of  $2650 \text{ kg/m}^3$  (siliciclastic material) and  $2230 \text{ kg/m}^3$  (pyroclastic material). The plot indicates that for each sediment type (pyroclastic or siliciclastic) the curve of  $C_{\min}$  versus  $T_f$  for an ambient water temperature  $T_a$  of  $12^{\circ}\text{C}$  is nearly the same as it is for an ambient water temperature  $T_a$  of  $24^{\circ}\text{C}$ . In the winter-spring season, when runs of series 1, 2, 3 and 4 were performed, temperature in the tank was  $12^{\circ}\text{C}$ . However, as shown on the plot of Figure 11, the difference between the corresponding lines is negligible.

It should be noted that the current cannot be expected to detach precisely when volume sediment concentration  $C$  becomes equal to  $C_{\min}$ . The current may run a short distance downstream under its own momentum before detaching.

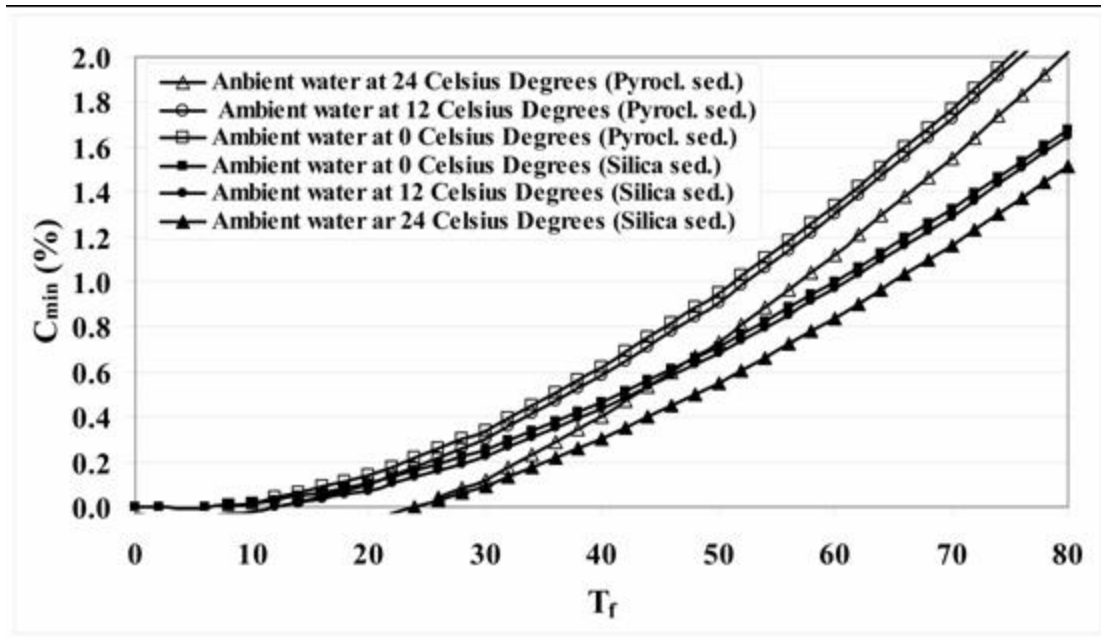


Figure 13. Minimum volume sediment  $C_{\min}$  concentration for a dense underflow as a function of temperature  $T_f$  of the water in the underflow for ambient temperatures  $T_a$  of 0, 12 and 24°C, and for siliciclastic and pyroclastic particulate material.

## 5 DISCUSSION AND IMPLICATIONS AT FIELD SCALE

Few subaerial volcanoes are constructed in single eruptions by repeated, high-temperature, density currents. The individual eruptions that produce tuff rings, for example, are driven by transfer of heat during magma-water interaction, resulting in relatively cool density currents, and current detachment hence has little effect on overall volcano morphology. In contrast, evidence suggests that deposition from repetitive, hot, eruption-fed density currents may play a controlling role in growth of some small volcanoes developed during short-lived underwater eruptions (e.g. Smellie & Hole, 1997; Mueller et al., 2000; Maicher, 2003). Such eruptions are not uncommon; they characterize for instance, the underwater phases of volcano construction in the 1963-65 Surtsey eruption sequence (Thorarinsson, 1967; White, 1996). Surtsey's submarine deposits have not been studied in detail, but a discontinuity in thickness of deposits from eruption-fed, hot, turbidity currents is inferred from some well-preserved volcanoes that were erupted into lakes. Pahvant Butte, which provided the samples for this study, and Black Point volcano, which erupted into the Pleistocene precursor of Mono Lake in California, are both inferred to have grown as mound-shaped, rather than cone-shaped, volcanoes during subaqueous phases of their eruptions (White, 1996; White, 2000); the flat-topped mounded shape of Black Point even led Christensen and Gilbert (1964) to suggest that this subaqueously erupted volcano indicated another possible origin for guyots. These mounds are constructed of shallow-dipping beds with ubiquitous current indicators and are inferred to have been formed largely by eruption-fed density currents of the sort examined in this experimental study. A notable feature of the mounds is that they do not appear to show the typical exponential thinning relationships expected for deposits formed either by settling from an eruption plume (Pyle, 1989) or deposition from simple dilute density currents (e.g. Sohn and Chough, 1989). Instead, the thick, coarse, and shallow-dipping beds of the mounds correlate over short distances with much finer-grained, widespread sheets of ash deposited by settling. Figure 10 illustrates this lateral transition at Black Point, where the effect was amplified by the volcano's growth into the path of glacier-fed

underflows. The two hundred metres of coarse-sand- to gravel- grade pyroclastic beds of the mound changes to only 10 metres of fine-medium sand grade ash over a distance of less than a kilometre. Pahvant Butte (White, 1996; 2001) shows a similar relationship, but is complicated because the mound was partly covered by a volcanic cone and derivative longshore spit that formed when the volcano built above lake level; its edges, like those of Black Point, were subsequently truncated by wave erosion when Lake Bonneville dropped to a lower level after the eruption.

The conclusion we draw from the form of these volcanoes, and the incongruity of shallow bedding dips within them, but abrupt transitions outward to thinner and finer-grained deposits, is that they owe their form in part to currents that exhibited some sort of threshold behavior in transport of the coarse volcanoclastic materials that comprise them. In light of the experimental results reported here, we suggest that the discontinuity reflects the detachment from the depositional surface of turbidity currents heated by their load of hot particles supplied by the eruption. At the point of current detachment, all bedload movement ceases, and suspended fines are lofted in a buoyant plume to the water's surface. Spreading of the plume controls distribution of ash settling to the depositional surface. Stacking of deposits from numerous turbidity currents builds a mound of pyroclastic beds consisting largely of fines-poor, bedload-deposited material. Finer ash from the eruption is largely partitioned into buoyant plumes arising either from the eruption column itself or, in the case investigated here, from detachment of warm eruption-fed density currents.

## 6 CONCLUSIONS

Subaqueous explosive volcanic eruptions inject dispersions of hot gas and particles into enclosing water. Heat transferred from the dispersions causes condensation of gas phases, producing heated aqueous dispersions. Gravity acts on the population of variably cooled, variably dense, pyroclastic particles to transform the dispersions into density currents, the runout, movement, and depositional behavior of which control the form of deposits, and thereby the edifices, produced by such eruptions.

In order to address the effects of variations in grain density and water temperature on flow properties and depositional processes, laboratory studies on density currents were performed at St. Anthony Falls Laboratory (University of Minnesota). Experiments were performed under a fixed set of flow conditions utilizing both pyroclastic material and silica sand that was sieved to a grain size distribution equivalent to the pyroclastic material. A series of runs in which a hot density current entered a cold environment, and a series in which a cold current entered a similarly cold environment were performed using each grain type. The deposits of the four sets of currents displayed a distinction based on density of the grains driving the current and the density contrast between the inflowing current and the ambient water.

The observed dynamics of the currents, and properties of the deposits produced, demonstrate that currents hotter than the ambient water display distinctive behaviors. In particular, a temperature gradient associated with a hot, sediment-laden current flowing into cold ambient water had the effects of a) reducing the streamwise head propagation velocity of the turbidity current, b) reducing the runout distance of the current and c) causing lofting of the turbidity current from the

channel bottom upward near the point of maximum runout to create a buoyant plume that spread and rose to the water surface.

The temperature difference also directly influenced deposit properties. For example, the center of mass of the deposit was located more proximally when a hot current entered a colder environment, whereas the center of mass was located distally when there was no temperature difference. In the case of a temperature difference, the resultant deposit showed two distinguishable zones. Upstream of the point of maximum runout the deposit was formed directly by the net-depositional turbidity current. The deposit downstream of this point consisted of grains that settled out of the buoyant plume.

Subaqueous edifice growth during the 1963-1965 Surtsey eruption in Icelandic waters, is inferred to have involved such heated currents, and products of similar eruptions into Pleistocene pluvial lakes in the western USA comprise fines-poor mound-shaped volcanoes with shallow-dipping internal layers and gentle upper slopes. Abrupt reduction in deposit thickness at the edge of the mounds characterizes their contact with the thin but widespread ash sheets that accompany them, and is interpreted to be the result of heated-current lofting, with the mound beds deposited from current bodies and bedload, and the ash sheets the product of suspension deposition from lofted plumes.

## 6 ACKNOWLEDGEMENTS

The research reported here was funded by the National Science Foundation through grant no. 0207303. Additional support was provided by the National Center for Earth-Surface Dynamics (NCED), a Science and Technology Center is funded by the National Science Foundation (NSF). JDL White also received support from the NZ Public Good Science Fund contract C05X0402 for part of this work. The authors are grateful to Bin Yu, Benjamin Erickson and Noel Abraham for help with the experiments.

## 7 REFERENCES

Allen, P. A. (1997) *Earth Surface Processes*. Blackwell Science, Oxford, 404 pp.

Busby-Spera, C. J. (1985) A sand-rich submarine fan in the lower Mesozoic Mineral King Caldera complex, Sierra Nevada, California. *J. sedim. Petrol.*, **55**, 376-391.

Busby-Spera, C. J. (1986) Depositional features of rhyolitic and andesitic volcanoclastic rocks of the Mineral King submarine caldera complex, Sierra Nevada, California. *J. volcanol. geotherm. Res.*, **27**, 43-76.

Chikita, K.A., Smith, N.D., Yonemitsu, N. and Perez-Arlucea, M., 1997. Dynamics of sediment-laden underflows passing over a subaqueous sill: glacier-fed Peyto Lake, Alberta, Canada. *Sedimentology*, 43: 865-875.

Chu, F.H., Pilkey, W.D. & Pilkey, O.H. 1979. An analytical study of turbidity current steady flow. *Mar. Geol.* 33, 205-220.

- Christensen, M. N. & Gilbert, C. M. (1964) Basaltic cone suggest constructional origin of some guyots. *Science*, 143, 240-242.
- Dickinson, W. R. (1968) Sedimentation of volcanoclastic strata of the Pliocene Koromavua Group in northwest Viti Levu, Fiji. *Am. J. Sci.*, **266**, 440-453.
- Ellison, T.H. & Turner, J.S. 1959 Turbulent entrainment in stratified flows. *J. Fluid Mech.* 6, 423-448.
- Fan J., Gijbels I. (1996) *Local Polynomial Modelling and Its Applications*. Chapman & Hall
- Fiske, R. S. (1963) Subaqueous pyroclastic flows in the Ohanapecosh Formation, Washington. *Bull. geol. Soc. Am.*, **74**, 391-406.
- Fiske, R. S., Cashman, K. V., Shibata, A. & Watanabe, K. (1998) Tephra dispersal from Myojinsho, Japan, during its shallow submarine eruption of 1952-1953. *Bull. Volcanol.*, **59**, 262-275.
- Garcia, M.H. 1985 Experimental study of turbidity currents. MS Thesis, Dept. of Civil and Mineral Engineering, University of Minnesota, USA.
- Gilbert, G.K., 1890. Lake Bonneville. United States Geological Survey Monograph, 1: 1-438.
- Hinze, J.O. 1960 On the hydrodynamics of turbidity currents. *Geol. Mijnb.* 39e, 18-25.
- Keulegan, G.H., 1957. An experimental study of the motion of saline water from locks into fresh water channels. US National Bureau of Standards Report, 5168.
- Lüthi, S. 1981 Some new aspects of two-dimensional turbidity currents. *Sedimentology* 28, 97-105.
- Maicher, D., 2003. A cluster of surtseyan volcanoes at Lookout Bluff, North Otago, New Zealand: Aspects of edifice spacing and time. In: J.D.L. White, J.L. Smellie and D.A. Clague (Editors), *Explosive Subaqueous Volcanism*. American Geophysical Union Monograph. American Geophysical Union, Washington DC, pp. 167-178.
- Maicher, D., White, J.D.L. and Batiza, R., 2000. Sheet hyaloclastite: density-current deposits of quench and bubble-burst fragments from thin, glassy sheet lava flows, Seamount Six, Eastern Pacific Ocean. *Marine Geology*, 171: 75-94.
- Manville, V., White, J.D.L., Houghton, B.F. and Wilson, C.J.N. 1998. The saturation behaviour of pumice and some sedimentological implications *Sed. Geol.*, 119: 5-16.
- Manville, V., Segschneider, B. and White, J.D.L., 2002. Hydrodynamic behaviour of Taupo 1800a pumice: implications for the sedimentology of remobilized pyroclasts. *Sedimentology*, 49(5): 955-976.

McLeod, P., Carey, S. & Sparks, R. S. J. (1999) Behaviour of particle-laden flows into the ocean: experimental simulation and geological implications. *Sedimentology*, **46**, 523-536.

Mueller, W.U., Garde, A.A. and Stendal, H., 2000. Shallow-water, eruption-fed, mafic pyroclastic deposits along a Paleoproterozoic coastline; Kangerluluk volcano-sedimentary sequence, Southeast Greenland. *Precambrian Research*, 101: 163-192.

Mueller, W. & White, J. D. L. (1992) Felsic fire-fountaining beneath Archean seas: pyroclastic deposits of the 2730 MA Hunter Mine Group, Quebec, Canada. *J. volcanol. geotherm. Res.*, **54**, 117-134.

Mulder, T. & Syvitski, J. P. M. (1995) Turbidity currents generated at river mouths during exceptional discharges to the world oceans. *J. Geol.*, **103**, 285-299.

Orton, G. J. (1996) Volcanic environments. In: *Sedimentary Environments: Processes, Facies and Stratigraphy* (Ed. by H. G. Reading), 485-567. Blackwell Science, Oxford

Parker, G. 1982 Conditions for the ignition of catastrophically erosive turbidity currents. *Mar. Geol.* 46, 307-327.

Plapp, J.E. & Mitchell, J. P. 1960 A hydrodynamic theory of turbidity currents. *J. Geophys. Res.* 65, 983-992.

Robertson, A. H. F. (1984) Mesozoic deep-water and Tertiary volcanoclastic deposition of Maio, Cape Verde Islands: Implications for Atlantic paleoenvironments and ocean island volcanism. *Bull. geol. Soc. Am.*, **95**, 433-453.

Smellie, J.L. and Hole, M.J., 1997. Products and processes in Pliocene-Recent, subaqueous to emergent volcanism in the Antarctic Peninsula: examples of englacial Surtseyan volcano construction. *Bulletin of Volcanology*, 58: 628-646.

Schmidt, W., 1911. *Zer Mechanik der Boen. Z. Meteorol.*, 28: 355-362.

Smellie, J. L. (1999) Subglacial Eruptions. In: *Encyclopedia of Volcanoes* (Ed. by H. Sigurdsson, B. F. Houghton, S. R. McNutt, H. Rymer and J. Stix), 403-418. Academic Press, San Diego, pp. 1417.

Stolzenbach, K. D. & Harleman, D. R. F. (1971) An analytical and experimental investigation of surface discharges of heated water. *Department of Civil Engineering Report*, **135**.

Stix J., Flow evolution of experimental gravity currents: implications for pyroclastic flows at volcanoes. *Journal of Geology*, 2001, 109, 381-398.

Von Karman, T., 1940. The engineer grapples with nonlinear problems. *Bulletin of the American Mathematical Society*, 46: 615-683.

Thorarinsson, S., 1967. Surtsey. The New Island in the North Atlantic. The Viking Press, New York, 47 pp.

Tilly, C. R. (1987) The sedimentology of the Taupo Pumice Alluvium Formation occurring in the lower region of the Hamilton Basin. Unpublished M.Sc., University of Waikato.

White, J.D.L. 2000. Subaqueous eruption-fed density currents and their deposits. In: Processes in physical volcanology and volcanoclastic sedimentation: modern and ancient Precambrian Res., 101: 87-109.

White, J.L. Smellie and D.A. Clague (Editors), Explosive Subaqueous Volcanism. American Geophysical Union Monograph. American Geophysical Union, Washington D.C.

White, J.D.L. 1996. Pre-emergent construction of a lacustrine basaltic volcano, Pahvant Butte, Utah (USA) Bull. Volcanol., 58: 249-262.

White, J.D.L., Manville, V., Wilson, C.J.N., Houghton, B.F., Riggs, N.R., Ort, M., 2001. Settling and deposition of 181 A.D. Taupo pumice in lacustrine and associated environments. International Association of Sedimentologists Special Publication, 30: 141-150.

White, J.D.L., Smellie, J.L. and Clague, D.A., 2003. Introduction: a deductive outline and topical overview of subaqueous explosive volcanism. In: J.D.L. White, J.L. Smellie and D.A. Clague (Editors), American Geophysical Union Monograph. Explosive Subaqueous Volcanism. American Geophysical Union, Washington D.C., pp. 1-20.

White, J. D. L. & Houghton, B. F. (1999) Surtseyan and related eruptions. In: *Encyclopedia of Volcanoes* (Ed. by H. Sigurdsson, B. Houghton, S. McNutt, H. Rymer and J. Stix), 495-512. Academic Press, New York, pp. 1427.

White, J. D. L., Manville, V., Wilson, C. J. N. & Houghton, B. F. (1997) Normal pumice. In: *General Assembly, International Association of Volcanology and Chemistry of the Earth's Interior*, p. 198, Puerto Vallarta, Mexico.

Whitham, A.G. and Sparks, R.S.J. 1986. Pumice Bull. Volcanol., 48: 209-223.

Gudmundsson, M.T. 2003. Melting of ice by magma-ice-water interactions during subglacial eruptions as an indicator of heat transfer in subaqueous eruptions. In: J.D.L.

Pantin, H.M. 1979 Interaction between velocity and effective density in turbidity flow: phase-plane analysis, with criteria for autosuspension. Mar. Geol. 31, 59-99.

## REFERENCES Non-CITED

- Batiza, R., Fornari, D. J., Vanko, D. A. & Lonsdale, P. (1984) Craters, calderas and hyaloclastites on young Pacific seamounts. *J. geophys. Res.*, **89**, 8371-8390.
- Cas, R. A. F. & Wright, J. V. (1987) *Volcanic Successions, Modern and Ancient*. Allen and Unwin, London, 528 pp.
- Cashman, K. V. & Fiske, R. S. (1991) Fallout of pyroclastic debris from submarine volcanic eruptions. *Science*, **253**, 275-280.
- Clarkson, R. A. (1996) Immediate post-c. 1800a Taupo eruption secondary deposits and shorelines. M.Sc., University of Otago.
- Colgate, S. A. & Sigurgeirsson, T. (1973) Dynamic mixing of water and lava. *Nature*, **244**, 552-555.
- Fisher, R. V. (1965) Settling velocity of glass shards. *Deep Sea Research*, **12**, 345-353.
- Fisher, R. V. & Schmincke, H.-U. (1984) *Pyroclastic Rocks*. Springer-Verlag, Berlin, 472 pp.
- Gladstone, C., Phillips, J. C. & Sparks, R. S. J. (1998) Experiments on bidisperse, constant volume gravity currents: propagation and sediment deposition. *Sedimentology*, **45**, 833-843.
- Julien, P. Y. (1995) *Erosion and Sedimentation*. Cambridge University Press, Cambridge, UK, 280 pp.
- Kneller, B. C. & Branney, M. J. (1995) Sustained high-density turbidity currents and the deposition of thick massive sands. *Sedimentology*, **42**, 607-616.
- Kokelaar, B. P. (1986) Magma-water interactions in subaqueous and emergent basaltic volcanism. *Bull. Volcanol.*, **48**, 275-289.
- Lowe, D. R. (1982) Sediment gravity flows: II. Depositional models with special reference to the deposits of high-density turbidity currents. *J. sedim. Petrol.*, **52**, 279-297.
- Maicher, D. (1996) A multiple vent sequence of a shallowing-up marine volcanoclastic complex at Lookout Bluff, New Zealand. In: *Western Pacific Geophysics Meeting, Brisbane, Australia EOS*, **77**, 126.
- Middleton, G. V. (1993) Sediment deposition from turbidity currents. *Annual Review of Earth and Planetary Sciences*, **21**, 89-114.
- Oehmig, R. & Wallrabe-Adams, H.-J. (1991) Hydrodynamic properties and grain-size characteristics of volcanoclastic deposits on the mid-Atlantic ridge north of Iceland (Kolbeinsey Ridge). *J. sedim. Petrol.*, **63**, 140-151.
- Postma, G., Nemeč, W. & Kleinspehn, K. L. (1988) Large floating clasts in turbidites: a mechanism for their emplacement. *Sediment. Geol.*, **58**, 47-61.
- Simpson, J. E. (1997) *Gravity currents in the environment and laboratory*. Cambridge University Press, Cambridge, 244 pp.
- Volcanoclastic density currents, p. 13 of 13*
- Smith, G. A. & Smith, R. D. (1985) Specific gravity characteristics of recent volcanoclastic sediment: implications for sorting and grain size analysis. *J. Geol.*, **93**, 619-622.
- Smith, T. L. & Batiza, R. (1989) New field and laboratory evidence for the origin of hyaloclastite flows on seamount summits. *Bull. Volcanol.*, **51**, 96-114.
- Wohletz, K. H. & Sheridan, M. F. (1983) Hydrovolcanic explosions II. Evolution of basaltic tuff rings and tuff cones. *Am. J. Sci.*, **283**, 384-413.

Wohletz, K. H. & McQueen, R. G. (1984) Experimental studies of hydromagmatic volcanism.  
In:  
*Explosive Volcanism; Inception, Evolution, and Hazards* (Ed. by P. o. e. volcanism), 158-  
169. National Academy Press, Washington, D.C.